An Optimal Primary Frequency Control Based on Adaptive Dynamic Programming for Islanded Modernized Microgrids

Masoud Davari, *Senior Member, IEEE*, Weinan Gao, *Member, IEEE*, Zhong-Ping Jiang, *Fellow, IEEE*, and Frank L. Lewis, *Life Fellow, IEEE*

***Abstract*—In many pilot research and development (R&D) microgrid projects, engine-based generators are employed in their power systems, either generating electrical energy or being mixed with the heat and power technology. One of the critical tasks of such engine-based generation units is the frequency regulation in the islanded mode of modernized microgrid (MMG) operation; MMGs are microgrids equipped with advanced controls to address more emerging scenarios in smart grids. For having a stable and reliable MMG, we need to synthesize an optimal, robust, primary frequency controller for the islanded mode of MMG of the future. This task is challenging because of unknown mechanical parameters, occurrence of uncertain disturbances, uncertainty of loads, operating point variations, and the appearance of engine delays, and hence nonminimum phase dynamics. This article presents an innovative primary frequency control for the engine generators regulating the frequency of an islanded MMG in the context of smart grids. The proposed approach is based on an adaptive optimal output-feedback control algorithm using adaptive dynamic programming (ADP). The convergence of algorithms, along with the stability analysis of the closed-loop system, is also shown in this article. Finally, as experimental validation, hardware-in-the-loop (HIL) test results are provided in order to examine the effectiveness of the proposed methodology practically.**

***Note to Practitioners*—This article was motivated by the problem of primary frequency controls in modernized microgrids (MMGs) using engine generators, which are still one of the prime sources of regulating frequency in pilot research and development (R&D) microgrid projects. Although MMGs will be integral parts of the smart grid of the future, their primary controls in the islanded mode are not advanced enough and not considering existing theoretical challenges scientifically. Existing approaches to regulate frequency using industrially accepted methods are highly model-based and not optimal. Besides, they are not considering the nonminimum phase dynamics. These dynamics are mainly associated with the engine delays—an inherent issue of mechanical parts—for islanded microgrids. This article suggests a new adaptive optimal output-feedback control approach based on the adaptive dynamic programming (ADP) to the abovementioned problem under consideration. By using the proposed methodology, MMGs can deal with the issues mentioned earlier, which are challenging. The proposed approach is optimally rejecting uncertain disturbances (considering the load uncertainty and operating point variations) and reducing the impacts of nonminimum phase dynamics caused by the engine delay. Based on our currently available hardware-in-the-loop (HIL) device's capability of modeling power systems' components in real time, our HIL-based experiments demonstrate that this approach is feasible.**

***Index Terms*—Adaptive dynamic programming (ADP), coupled dynamics, engine delay, hardware-in-the-loop (HIL) islanded mode of modernized microgrids (MMGs), nonminimum phase zero dynamics, output-feedback control, primary frequency control, smart modernized grids, uncertain.**

Nomenclature

K^*	Optimal state-feedback control gain.
$\mathcal{K}_j$	Output-feedback control gain learned at iteration j.
ν	Stopping criterion of Algorithms 1 and 2.
ω_e	Electrical frequency for electrical variables.
ω_r	Mechanical frequency (or equivalently rotor speed).
ω_s	System base frequency for electrical variables.
$\Psi_{d/q}$	d/q-axis of the flux linkage matrix of the machine.
$\psi_{d/q}$	Per-unitized value of $\Psi_{d/q}$.
A_c	State matrix of continuous-time system (3).
A_d	State matrix of discrete-time system (4).
B_c	Input matrix of continuous-time system (3).
B_d	Input matrix of discrete-time system (4).
C	Output matrix of continuous-time system (3).
D	Friction coefficient.
E_c	Disturbance input matrix of continuous-time system (3).
E_d	Disturbance input matrix of discrete-time system (4).
$I_{d/q}$	d/q-axis of the current matrix of the machine.

Manuscript received December 5, 2019; revised March 4, 2020; accepted April 21, 2020. Date of publication June 3, 2020; date of current version July 2, 2021. This article was recommended for publication by Associate Editor S. Dadras and Editor Q. Zhao upon evaluation of the reviewers' comments. This work was supported by the U.S. National Science Foundation (NSF) awards through the Core Program of Energy, Power, Control, and Networks in the Division of Electrical, Communications and Cyber Systems (ECCS) under Grant #1808279, Grant #1902787, and Grant #1903781. *(Corresponding author: Weinan Gao.)*

Masoud Davari and Weinan Gao are with the Department of Electrical and Computer Engineering, Allen E. Paulson College of Engineering and Computing, Georgia Southern University (Statesboro Campus), Statesboro, GA 30460 USA (e-mail: mdavari@georgiasouthern.edu; wgao@georgiasouthern.edu).

Zhong-Ping Jiang is with the Department of Electrical and Computer Engineering, Tandon School of Engineering, New York University, Brooklyn, NY 11201 USA (e-mail: zjiang@nyu.edu).

Frank L. Lewis is with the UTA Research Institute, The University of Texas at Arlington, Fort Worth, TX 76118 USA (e-mail: lewis@uta.edu).

Color versions of one or more of the figures in this article are available online at https://ieeexplore.ieee.org.

Digital Object Identifier 10.1109/TASE.2020.2996160

I_f	Field current in the rotor winding.
I_{kd}	Current in the rotor winding kd ("kd" refers to the quantities related to the k damper windings of the d-axis.
I_{mq}	Current in the rotor winding mq ("mq" refers to the quantities related to the m damper windings of the q-axis.
J	Combined moment of inertia of machine and turbine.
j	Learning iteration.
$\mathcal{K}^*$	Optimal output-feedback control gain.
K_j	State-feedback control gain learned at iteration j.
$L_{\epsilon d}$	Leakage inductance of d-winding.
$L_{\epsilon q}$	Leakage inductance of q-winding.
$L_{d/q}$	d/q-axis of the inductance matrix of the machine.
L_{ld}	$L_d - L_{\epsilon d}$.
L_{lq}	$L_q - L_{\epsilon q}$.
r_s	Both d- and q-axis of the resistance matrix of the machine.
T_e	Electrical torque developed by the machine.
T_m	Mechanical torque applied to the machine axis.
$V_{d/q}$	d/q-axis of the voltage matrix of the machine.

I. Introduction

The energy sector has been significantly progressing and moving toward simultaneously integrating more distributed energy resources (DERs), in the shape of either engine-based generations or renewables, power networks, and energy storage systems (e.g., battery systems) under the umbrella of smart grids [1]–[3]. In the smart grid paradigm, the modernized microgrid (MMG) concept brings many benefits to the control, operation, and demand supply within the electric power industry. MMGs are microgrids equipped with advanced controls to address more emerging scenarios in smart grids. One of the essential elements in smart, modernized grids is having more advanced, sophisticated, modern controls, along with communications, as per the Energy Independence and Security Act of 2007 (EISA-2007), which was approved by the U.S. Congress in January 2007 and signed into law in December 2007 [4]. Microgrid hierarchical controls have various time intervals and horizons—ranging from milliseconds (i.e., inner control loop and the primary controls), milliseconds to seconds (i.e., secondary controls), and seconds to minutes (i.e., tertiary controls). They are detailed as follows. Inner control loops, as well as the primary controls, are regulating the voltage and frequency to their reference values. The secondary control is adjusting the deviations in both voltage and frequency. The tertiary control manages the power flow by regulating amplitude voltage and frequency when the MMG is connected to the grid.

One of the vital MMGs' operation modes is the islanded mode [5], which requires MMG to control the frequency of the grid under its territory. In this regard, various frequency control methods of different hierarchical levels (i.e., primary, secondary, or tertiary level of frequency controls) are being involved in and playing an integral role in the expansion, implementation, and modernization of currently operating microgrids and power systems. As a result, we need to make the primary frequency control of MMGs more reliable and robust. This initiative impacts the whole dynamic system as it is the most inner loop from the perspective of the entire closed-loop dynamic system and, hence, the overall stability. Among different DERs having the responsibility of primary frequency control, engine-based DERs are still being used in many pilot microgrid projects and research and development (R&D) of the energy industry. For example, they have been part of BC Hydro Boston Bar island, Senneterre substation, The Consortium for Electric Reliability Technology Solutions (CERTS) microgrid, and the Illinois Institute of Technology (IIT) microgrid (see [3] and references therein).

As detailed in [3], engine generators are still being utilized in university campuses and hospitals for controlling the frequency of their islanded grid territories. Consequently, to this end, MMGs of the future will employ engine generators in their power systems as well. The engine-based generators are also applied in naval power systems as the primary source of generation [6]. Their dynamics need special consideration from the standpoint of both adaptive and optimal controls because of the following points.

1) The transient frequency response of the islanded power system needs to be optimized from the perspective of performance while considering the energy of the error—will see the cost function in (11).
2) The parameters of their dynamic systems are uncertain from the fact that many mechanical parameters are not precisely measurable, so they are within a predefined range.
3) Some uncertain disturbances are coming from the fast dynamics of electrical variables, such as voltage control loops, and hence field control loops.
4) The load works as a direct uncertain disturbance impacting the output performance abruptly.
5) The resultant dynamics are uncertain since they have been linearized around an operating point.
6) Due to load variations, the frequency of an MMG will fluctuate in a wide range because of the limited values of rotational inertia of the prime movers and generators.
7) There is a delay associated with the engine response in the open-loop dynamics, so it resulted in nonminimum phase zeros reducing and impacting phase margin of the closed-loop dynamics dramatically.

Therefore, the issues stated earlier can dramatically impact on the frequency regulation of MMGs, especially during the islanded mode, and hence the protections and other control functionalities accordingly. In order to tackle these issues—considering practical aspects of both power and control disciplines—this article addresses an adaptive optimal frequency control design for an engine-based generator with assured disturbance rejection and tracking ability. The method proposed in this article can be generalized to other technologies for regulating frequency, although they are not the main scope of this article. In case new technologies are employed, e.g., renewables and batteries, they are indeed required to have reasonable inertia, which is "virtually" implemented in their controls. This topic is a separate field of study,

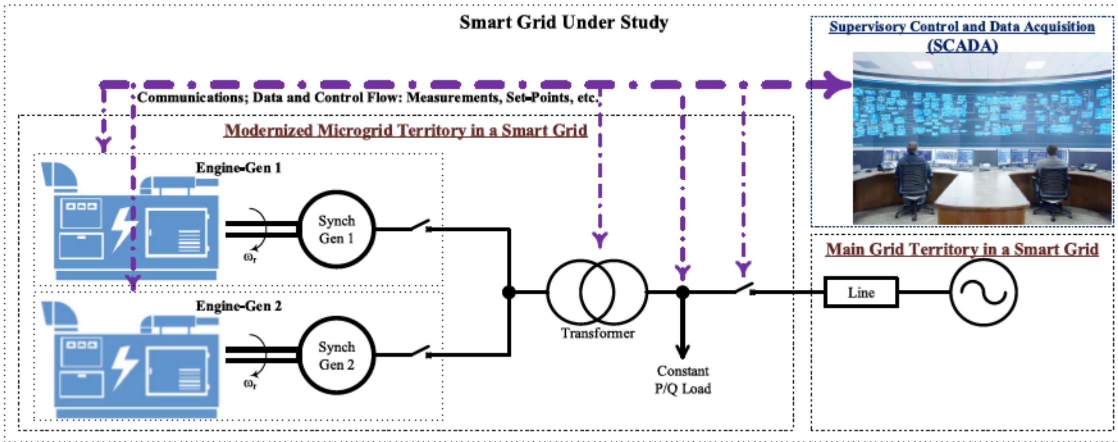

Fig. 1. Islanded MMG energized by two paralleled engine generators.

which needs to be studied in comprehensive research. For example, the researchers in [7] and [8] have detailed the implementation of the virtual inertia in power-electronic-based systems without any mechanical inertia. Last but not least, from the standpoint of frequency dynamics, there will be a dynamic mode similar to what has been derived in this article.

In control engineering, the asymptotic tracking with disturbance rejection problem, named output regulation problem, has been studied since the 1970s [9]. Nonetheless, a common feature of these publications is that they have not addressed optimal solutions. The model-based linear optimal output regulation problem has been studied for the sake of enhancing the transient response of dynamical systems (see [10] and references therein). However, the optimal control policies proposed in these articles usually assume the precise knowledge of the control system in question. Approximate/adaptive dynamic programming (ADP) is a practically sound, data-driven approach that provides a way to solve the adaptive and optimal control problem in a successive iterative fashion. Essentially, it is an adaptive optimal control method that can approximate the optimal controller via online/real-time data [11]–[19]. Recently, ADP and the internal model principle have combined to study the leader-to-formation stability of uncertain multiagent systems [20].

This article, for the first time, proposes a measurement-feedback adaptive optimal control design approach for the output regulation problem of uncertain linear systems via internal model principle. Then, we apply the proposed control approach [via hardware-in-the-loop (HIL)-based testing] to the frequency regulation of MMGs. The contributions of this article are listed as follows. First, the frequency regulation problem in the applications mentioned earlier is formulated in state-space representation applicable to the ADP design problem while considering all influential dynamics and disturbance. Second, this article solves the control problem with completely unknown plant and exosystem dynamics, which is well matched with the existing problems under study for MMGs.

Furthermore, the closed-loop systems with optimal control strategies obtained by minimizing the quadratic performance index generally have satisfactory transient performance. Third, different from ADP methods with full-state accessibility [17], [21], the proposed approach utilizes only measurement feedback and considers the input time delay. This methodology is well designed to be applicable to control a large number of practical systems arising from power systems for which the state is not measurable. Fourth, the proposed ADP approach is based on a value iteration (VI). Different from the policy iteration approach, the proposed learning strategy does not rely on the knowledge of the initial possible control policy.

The remainder of this article is organized as follows. We formulate the dynamic model of the frequency control loop of an engine generator in an islanded mode of MMG's operation in Section II. Then, we propose an adaptive optimal control approach via output feedback and internal model in Section III. As an experimental validation process, we practically examine the proposed method on an example of an islanded MMG using a real-time simulation platform as an HIL testing in Section IV. Finally, Section V contains the conclusions and future research work.

Notations: Throughout this article, $|\cdot|$ represents the Euclidean norm for vectors and the induced norm for matrices. $\otimes$ indicates the Kronecker product operator. $\text{vec}(A) = [a_1^T, a_2^T, \ldots, a_m^T]^T$, where $a_i \in \mathbb{R}^n$ are columns of $A \in \mathbb{R}^{n\times m}$. For a symmetric matrix $P \in \mathbb{R}^{m\times m}$ and a column vector $\upsilon \in \mathbb{R}^n$, operators vecs and vecv denote $\text{vecs}(P) = [p_{11}, 2p_{12}, \ldots, 2p_{1m}, p_{22}, 2p_{23}, \ldots, 2p_{m-1,m}, p_{mm}]^T \in \mathbb{R}^{(1/2)m(m+1)}$, and $\text{vecv}(\upsilon) = [\upsilon_1^2, \upsilon_1\upsilon_2, \ldots, \upsilon_1\upsilon_n, \upsilon_2^2, \upsilon_2\upsilon_3, \ldots, \upsilon_{n-1}\upsilon_n, \upsilon_n^2]^T \in \mathbb{R}^{(1/2)n(n+1)}$.

II. Modeling the Detailed Frequency Dynamics of an Islanded MMG

In this section, we model an islanded power system in the context of MMG benefiting from two paralleled engine generators, as shown in Fig. 1, without loss of generality of this problem. In Fig. 1, an islanded MMG feeding electric

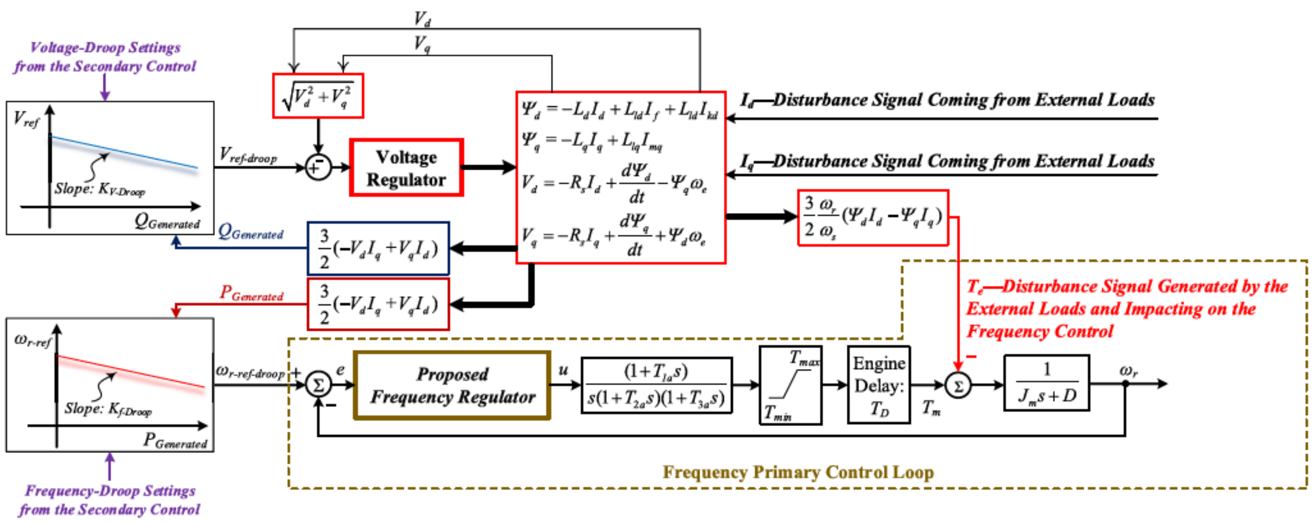

Fig. 2. Detailed dynamics of the primary frequency control of an engine-generator within an islanded MMG paradigm in the d/q-frame—the proposed frequexcy regulator has been detailed in Fig. 3(b).

load has been demonstrated. It is noteworthy that in order to extract the model of the frequency dynamics and formulate the problem, the authors have benefited from previous works in this field (see [22]–[24] and references therein). Based on them, as shown in Fig. 2, (1) describes the details of the dynamic model used in the primary frequency controls. Also, it should be stated that if other new technologies (e.g., renewables and batteries) are used, based on the requirement of implementing virtual inertia (see [7], [8]), a dynamic model similar to (1) will be derived for the frequency dynamics in islanded MMGs

$$\dot{\omega}_r = \frac{1}{J}(T_m - T_e - D\omega_r)$$
$$T_e = \frac{3}{2}\frac{\omega_r}{\omega_s}(\Psi_d I_d - \Psi_q I_q). \tag{1}$$

Fig. 2 briefly shows the dynamics of different related variables of (1) in the d/q-frame. Different parameters of the engine generator dynamics shown in Fig. 2 have been detailed in the Nomenclature.

For making Fig. 2 concise, we did not include all quantities associated with the k damper windings of the d-axis and related to the m damper windings of the q-axis, such as their associated flux linkages and the voltages, i.e., Ψ_{kd}, Ψ_{mq}, V_{kd}, and V_{mq}. However, they have been considered (see [22]–[24], and references therein).

In this article, the time delay is approximated by a nonminimum phase system whose transfer function $H(s)$ is

$$H(s) = \frac{1 - 0.5T_D s}{1 + 0.5T_D s}. \tag{2}$$

From (1) and Fig. 2, one can formulate the frequency control problem in a state-space representation as follows (see the Appendix for detail):

$$\dot{x}(t) = A_c x(t) + B_c u(t) + E_c T_e(t)$$
$$e(t) = Cx(t) + \omega_{r\text{-ref}-\text{droop}} \tag{3}$$

where the state $x \in \mathbb{R}^5$, the input u is shown in Fig. 2, the output $y(t) = Cx(t) := -\omega_r(t)$, and the disturbance input T_e is a piecewise constant function—which means that it remains constant over the sampling period. It is noteworthy that it considers all intermittent renewables as their rate of change is much slower than our sampling interval. Consequently, this presumption is reasonable for the scope of our modeling. This assumption does not change the generality of the proposed method. It is checkable that the pair (A_c, B_c) is controllable and (C, A_c) is observable.

III. Controller Design

In this section, we develop an adaptive optimal control approach for the power system via output feedback. First, a state reconstruction method is presented in terms of sampled input and output. Then, a data-driven adaptive optimal control strategy is proposed in terms of ADP and VI.

A. System Discretization

Choosing a nonpathological sampling period T_s [25], the continuous-time system (3) can be discretized as follows:

$$x_{k+1} = Ax_k + Bu_k + Ev_k$$
$$z_{k+1} = z_k + e_k$$
$$e_k = Cx_k + Fv_k \tag{4}$$

where $v_k = [(T_e)_k, (\omega_{r-\text{ref}-\text{droop}})_k]^T$, and system matrices are $A = e^{A_c T_s}$, $B = (\int_0^{T_s} e^{A_c \tau} d\tau) B_c$, $E = (\int_0^{T_s} e^{A_c \tau} d\tau) E_c [1\ 0]$, and $F = [0\ 1]$. The state z_k stands for the summation of the error. Noticing that the sampling frequency is much higher than the rate of the load variation (or equivalently disturbance T_e), it is reasonable to treat v as a constant during each sampling interval. In this way, (4) satisfies internal model principle [9]. The following mild assumption is made for developing the controller.

Assumption 1: The transmission zeros condition holds, that is

$$\text{rank}\begin{bmatrix} A-I & B \\ C & 0 \end{bmatrix} = n+1. \tag{5}$$

The output regulation problem finds a controller such that the closed-loop system is asymptotically stable with the tracking error $\lim_{k\to\infty} e_k = 0$. The following lemma shows that the control problem can be solved by developing a state-feedback controller.

Lemma 1: Under Assumption 1, choose the control gains K_x and K_z such that $\begin{bmatrix} A - BK_x & -BK_z \\ C & 1 \end{bmatrix}$ is a Schur matrix. Then, the system (4) with $u_k = -K_x x_k - K_z z_k$ is exponentially stable with $\lim_{k\to\infty} e_k = 0$.

Proof: Based on Assumption 1, there always exist a unique vector $X \in \mathbb{R}^n$ and a constant $U \in \mathbb{R}$ solving the following matrix equations:

$$X = AX + BU + E \tag{6}$$
$$0 = CX + F. \tag{7}$$

Moreover, from [26, Lemma 1.38], there always exist a unique solution $(\hat{X}, Z)$ solving (7) and

$$\begin{bmatrix} X \\ Z \end{bmatrix} = \begin{bmatrix} A - BK_x & -BK_z \\ C & 1 \end{bmatrix} \begin{bmatrix} X \\ Z \end{bmatrix} + \begin{bmatrix} E \\ 0 \end{bmatrix}. \tag{8}$$

Therefore, we have $X = \hat{X}$ and $U = -K_x X - K_z Z$. Letting $\bar{x}_k = x_k - X\upsilon_k$, $\bar{z}_k = z_k - Z\upsilon_k$, and

$$\bar{u}_k = u_k - U\upsilon_k := -K_x\bar{x}_k - K_z\bar{z}_k \tag{9}$$

then the system (4) can be transformed by

$$\begin{aligned} \begin{bmatrix} \bar{x}_{k+1} \\ \bar{z}_{k+1} \end{bmatrix} &= \begin{bmatrix} A & 0 \\ C & 1 \end{bmatrix} \begin{bmatrix} \bar{x}_k \\ \bar{z}_k \end{bmatrix} + \begin{bmatrix} B \\ 0 \end{bmatrix} \bar{u}_k \\ &:= \bar{A}w_k + \bar{B}\bar{u}_k \\ e_k &= C\bar{x}_k. \end{aligned} \tag{10}$$

It is checkable that the system (10) with (9) is exponentially stable at the origin, which indicates that $\lim_{k\to\infty} \bar{x}_k = 0$ and $\lim_{k\to\infty} \bar{u}_k = 0$, and $\lim_{k\to\infty} e_k = 0$. The proof is thus completed. □

B. Model-Based State-Feedback Optimal Controller Design

In this article, we expect the designed controller cannot only reject the disturbance but also improve the transient performance through minimizing the following cost function:

$$\begin{aligned} &\min_{\bar{u}_k} \sum_{k=0}^{\infty} Q_1 e_k^2 + Q_2 \bar{z}_k^2 + R\bar{u}_k^2 \\ &\text{s.t. } (10) \end{aligned} \tag{11}$$

where Q_1, Q_2, and R are positive constants.

By a linear optimal control theory, the optimal controller that minimizes (11) is

$$\bar{u}_k = -K_x^* \bar{x}_k - \bar{K}_z^* \bar{z}_k = -K^* w_k \tag{12}$$

which is equivalent to $u_k = -K^*[x_k^T \; z_k]^T$.

Letting $\bar{Q} = \begin{bmatrix} C^T Q_1 C & 0 \\ 0 & Q_2 \end{bmatrix}$, then the optimal feedback control gain is

$$K^* = (R + \bar{B}^T P^* \bar{B})^{-1} \bar{B}^T P^* \bar{A}$$

where the constant matrix $P^* = (P^*)^T > 0$ uniquely solves the following discrete-time algebraic Riccati equation (ARE):

$$\bar{A}^T P \bar{A} - P + \bar{Q} - \bar{A}^T P \bar{B}(R + \bar{B}^T P \bar{B})^{-1} \bar{B}^T P \bar{A} = 0. \tag{13}$$

C. Value Iteration

We see that the optimal state-feedback controller design relies on the solution to ARE (13) that is nonlinear in P. However, solving it, directly, is often hard, especially for high-dimensional dynamical systems. The VI algorithm 1 developed in [27] is able to approximate the solution to (13) with assured convergence.

Algorithm 1 VI Algorithm [27]

1: $j \leftarrow 0$. $P_j \leftarrow 0$. Select a threshold $\nu > 0$.

2: **repeat**

$$\begin{aligned} P_{j+1} &\leftarrow \bar{A}^T P_j \bar{A} - \bar{A}^T P_j \bar{B} \\ &\quad \times (R + \bar{B}^T P_j \bar{B})^{-1} \bar{B}^T P_j \bar{A} + \bar{Q} \end{aligned} \tag{14}$$

$$\begin{aligned} K_{j+1} &\leftarrow (R + \bar{B}^T P_{j+1} \bar{B})^{-1} \bar{B}^T P_{j+1} \bar{A} \\ j &\leftarrow j + 1 \end{aligned} \tag{15}$$

3: **until** $|P_j - P_{j-1}| < \nu$

It is shown in [27, Lemma 17.5.4] that, for $j = 0, 1, 2, \ldots$, considering P_j and K_j defined in (14) and (15), the following properties hold.

1) $P^* \geq P_{j+1} \geq P_j$.
2) $\lim_{j\to\infty} K_j = K^*$, $\lim_{j\to\infty} P_j = P^*$.

Therefore, when the model is perfectly known and the state is available, one can use the model-based Algorithm 1 to approximate the optimal state-feedback control gain K^*. We are going to show an output-feedback optimal controller design through state reconstruction when the state is unavailable.

D. Model-Based Output-Feedback Optimal Controller Design

The dynamics of (10) can be written on a time horizon $[k - n, k - 1]$ as the expanded state and output equations

$$\begin{aligned} \bar{x}_k &= A^n x_{k-n} + \mathcal{C}_1 \tilde{u}_{k-1,k-n} \\ \tilde{e}_{k-1,k-n} &= \mathcal{O} x_{k-n} + \mathcal{T} \tilde{u}_{k-1,k-n} \end{aligned} \tag{16}$$

where vectors

$$\begin{aligned} \tilde{u}_{k-1,k-n} &= [\bar{u}_{k-1}, \bar{u}_{k-2}, \ldots, \bar{u}_{k-n}]^T \in \mathbb{R}^n \\ \tilde{e}_{k-1,k-n} &= [e_{k-1}, e_{k-2}, \ldots, e_{k-n}]^T \in \mathbb{R}^n \end{aligned}$$

and matrices

$$\mathcal{C} = [B, A\,B, \ldots, A^{n-1}B] \in \mathbb{R}^{n\times n}$$
$$\mathcal{O} = [(CA^{n-1})^T, \ldots, (CA)^T, C^T]^T \in \mathbb{R}^{n\times n}$$
$$\mathcal{T} = \begin{bmatrix} 0 & CB & CAB & \cdots & CA^{n-2}B \\ 0 & 0 & CB & \cdots & CA^{n-3}B \\ \vdots & \vdots & \ddots & \ddots & \vdots \\ 0 & 0 & \cdots & 0 & CB \\ 0 & 0 & 0 & 0 & 0 \end{bmatrix} \in \mathbb{R}^{n\times n}.$$

Since the sampling period is non-pathological, we have that the pair (A, B) is controllable and (C, A) is observable, which implies that the observability matrix $\mathcal{O}$ is always invertible. Therefore, the state $\bar{x}_k$ can be reconstructed uniquely by the retrospective input and measurement output information, i.e., $\bar{x}_k = M\chi_k$ with

$$M = [A^n\mathcal{O}^{-1}, \mathcal{C} - A^n\mathcal{O}^{-1}\mathcal{T}] \in \mathbb{R}^{n\times 2n}$$
$$\chi_k = [\bar{e}_{k-1,k-n}^T, \bar{u}_{k-1,k-n}^T]^T \in \mathbb{R}^{2n}.$$

From (18), one can see that the optimal controller (12) is equivalent to the following output-feedback controller:

$$\bar{u}_k = -\mathcal{K}_x^*\chi_k - K_z^*\bar{z}_k := -\mathcal{K}^*\boldsymbol{w}_k \tag{17}$$

where $\mathcal{K}_x^* = K_x^*M$. Moreover, we have

$$\boldsymbol{w}_k = \begin{bmatrix} M & 0 \\ 0 & 1 \end{bmatrix} w_k := \mathcal{M}w_k. \tag{18}$$

However, the optimal control policy designed in this way is essentially model-based, which relies on the perfect knowledge of system model. Due to parametric variations or unmodeled dynamics, it is usually hard to know the exact model of a power system. We will design data-driven control approaches in the absence of the precise knowledge of the dynamic model. The optimal controller can be learned using online input and output data.

E. Output-Feedback Adaptive Optimal Controller Design

In this section, we will propose a data-driven adaptive optimal control approach for frequency control of power system with unknown system dynamics and unmeasurable state $\bar{x}_k$.

Based on the error system (10) and (14), we have

$$\begin{aligned}
&\begin{bmatrix} w_k \\ \bar{u}_k \end{bmatrix}^T \begin{bmatrix} \bar{Q} + \bar{A}^T P_{j+1}\bar{A} & \bar{A}^T P_{j+1}\bar{B} \\ \bar{B}^T P_{j+1}\bar{A} & R + \bar{B}^T P_{j+1}\bar{B} \end{bmatrix} \begin{bmatrix} w_k \\ \bar{u}_k \end{bmatrix} \\
&= \begin{bmatrix} w_{k+1} \\ -K_j w_{k+1} \end{bmatrix}^T \begin{bmatrix} \bar{Q} + \bar{A}^T P_j\bar{A} & \bar{A}^T P_j\bar{B} \\ \bar{B}^T P_j\bar{A} & R + \bar{B}^T P_j\bar{B} \end{bmatrix} \\
&\quad \begin{bmatrix} w_{k+1} \\ -K_j w_{k+1} \end{bmatrix} + Q_1 e_k^2 + Q_2\bar{z}_k^2 + R\bar{u}_k^2.
\end{aligned} \tag{19}$$

One can obtain the following equation based on the state reconstruction results:

$$\begin{aligned}
\begin{bmatrix} \boldsymbol{w}_k \\ \bar{u}_k \end{bmatrix}^T \mathcal{P}_{j+1} \begin{bmatrix} \boldsymbol{w}_k \\ \bar{u}_k \end{bmatrix} &= Q_1 e_k^2 + Q_2\bar{z}_k^2 + R\bar{u}_k^2 \\
&\quad + \begin{bmatrix} \boldsymbol{w}_{k+1} \\ \bar{u}_{k+1} \end{bmatrix}^T \mathcal{P}_j \begin{bmatrix} \boldsymbol{w}_{k+1} \\ \bar{u}_{k+1} \end{bmatrix} := \phi_k^j
\end{aligned} \tag{20}$$

where

$$\begin{aligned}
\mathcal{P}_j &= \begin{bmatrix} \mathcal{M}^T(\bar{Q} + \bar{A}^T P_j\bar{A})\mathcal{M} & \mathcal{M}^T\bar{A}^T P_j\bar{B} \\ \bar{B}^T P_j\bar{A}\mathcal{M} & R + B^T P_j B \end{bmatrix} \\
&:= \begin{bmatrix} \mathcal{P}_j^{11} & \mathcal{P}_j^{12} \\ \mathcal{P}_j^{21} & \mathcal{P}_j^{22} \end{bmatrix} \\
\mathcal{K}_j &= K_j\mathcal{M}.
\end{aligned} \tag{21}$$

Given a sufficiently large positive integer s and a sequence $\{a_k\}_{k=0}^{\infty}$, where $a_k \in \mathbb{R}^{n_a}$, define

$$\Gamma(a_k) = [\text{vecv}(a_{k_0}), \text{vecv}(a_{k_0+1}), \ldots, \text{vecv}(a_{k_0+s})]^T$$

with $k_0 > n$. Let

$$\Theta = \Gamma\left(\begin{bmatrix} \boldsymbol{w}_k \\ \bar{u}_k \end{bmatrix}\right).$$

For $j = 0, 1, 2, \ldots$ we define

$$\Phi_j = \left[\phi_{k_0}^j, \phi_{k_0+1}^j, \ldots, \phi_{k_0+s}^j\right]^T.$$

Then, (20) implies

$$\Theta\text{vecs}(\mathcal{P}_{j+1}) = \Phi_j. \tag{22}$$

The VI-based ADP algorithm is proposed in Algorithm 2, which does not rely on an initial stabilizing control gain.

Algorithm 2 VI-Based Measurement Feedback ADP Algorithm

Select a threshold $\nu > 0$. $j \leftarrow 0$
Apply an arbitrary control policy on $[0, k_0 + s]$
repeat
    Solve $\mathcal{P}_{j+1}$ from (22)
    Solve $\mathcal{K}_{j+1}$ by

$$\mathcal{K}_{j+1} \leftarrow (\mathcal{P}_{j+1}^{22})^{-1}\mathcal{P}_{j+1}^{21} \tag{23}$$

    $j \leftarrow j + 1$
until $|\mathcal{P}_j - \mathcal{P}_{j-1}| < \nu$
$j^* \leftarrow j$. Obtain the approximated optimal control gain $\mathcal{K}_{j^*}$

We will state a result on the convergence of the proposed Algorithm 2.

Theorem 1: Sequences $\{\mathcal{P}_j\}_{j=1}^{\infty}$ and $\{\mathcal{K}_j\}_{j=2}^{\infty}$ obtained from solving Algorithm 2 converge to $\mathcal{P}^*$ and $\mathcal{K}^*$, where

$$\begin{aligned}
\mathcal{P}^* &= \begin{bmatrix} \mathcal{M}^T(\bar{Q} + \bar{A}^T P^*\bar{A})\mathcal{M} & \mathcal{M}^T\bar{A}^T P^*\bar{B} \\ \bar{B}^T P^*\bar{A}\mathcal{M} & R + B^T P^* B \end{bmatrix} \\
\mathcal{K}^* &= (\mathcal{P}^{22})^{-1}\mathcal{P}^{21}.
\end{aligned} \tag{24}$$

Proof: Given any symmetric matrix P_j, $P_{j+1} = P_{j+1}^T$ and K_{j+1} are uniquely determined by (14) and (15). One can check that the corresponding matrices $\mathcal{P}_{j+1}$ and $\mathcal{K}_{j+1}$ defined in (21) satisfy (22) and (23). If $\mathcal{P}$ and $\mathcal{K}$ solve (22) and (23), then we immediately have $\mathcal{P} = \mathcal{P}_{j+1}$ and $\mathcal{K} = \mathcal{K}_{j+1}$. Since $\mathcal{P}$ and $\mathcal{K}$ are unique under the full-rank condition, $\mathcal{P}_{j+1} = \mathcal{P}$ and $\mathcal{K}_{j+1} = \mathcal{K}$ are uniquely determined. Given property 2) in Algorithm 1, we have $\lim_{j\to\infty}\mathcal{P}_j = \mathcal{P}^*$, $\lim_{j\to\infty}\mathcal{K}_j = \mathcal{K}^*$. □

Afterward, we show the closed-loop system stability in the following theorem.

Theorem 2: Given a control gain $\mathcal{K}_j^*$ learned from Algorithm 2. The control policy

$$\bar{u}_k = -\mathcal{K}_j^*\boldsymbol{w}_k \tag{25}$$

exponentially stabilizes the system (4) and $\lim_{k\to\infty} e_k = 0$.

Proof: Based on the state reconstruction shown in Section III-D, it is checkable that (25) is equivalent to

$\bar{u}_k = -K_x^{j*}\bar{x}_k - \bar{K}_z^{j*}\bar{z}_k$, and the system (4) in closed loop with the approximated controller satisfies

$$\begin{bmatrix}\bar{x}_{k+1}\\ \bar{z}_{k+1}\end{bmatrix} = \begin{bmatrix}A - BK_x^{j*} & -BK_z^{j*}\\ C & 1\end{bmatrix}\begin{bmatrix}\bar{x}_k\\ \bar{z}_k\end{bmatrix} := \bar{A}_c\begin{bmatrix}\bar{x}_k\\ \bar{z}_k\end{bmatrix}$$
$$e_k = C\bar{x}_k. \tag{26}$$

From Theorem 1, there always exists a small enough threshold $\nu > 0$ in Algorithm 2 such that $\bar{A}_c$ is a Schur matrix, which implies that $\lim_{k\to\infty}\bar{x}_k = 0$ and $\lim_{k\to\infty}\bar{z}_k = 0$. Then, we have $\lim_{k\to\infty} e_k = \lim_{k\to\infty} C\bar{x}_k = 0$. The proof is thus completed. □

Besides stability, one can analyze the suboptimality of the developed control policy (25), which has been shown as follows.

Theorem 3: Let $J^\dagger$ be the cost for the system (4) in closed loop with the approximate optimal control policy (25). Let J^* be the cost for the system (4) with the optimal control policy (12). There exists a positive number μ such that $\mu J^\dagger \leq J^*$.

Proof: The system (4) in closed loop with (25) satisfies (26), which is equivalent to

$$w_{k+1} = \bar{A}_c w_k := \left(\bar{A} - \bar{B}K_j^*\right)w_k \tag{27}$$

where $K_j^* = \left[K_x^{j*}\ \bar{K}_z^{j*}\right]$.

Since $\bar{A}_c$ is a Schur matrix, there exists a positive-definite matrix $P^\dagger$ solving the following Lyapunov equation:

$$\bar{A}_c^T P^\dagger \bar{A}_c - \bar{A}_c + \begin{bmatrix}Q_1 & 0\\ 0 & Q_2\end{bmatrix} + \left(K_j^*\right)^T RK_j^* = 0. \tag{28}$$

Therefore, it can be obtained that the cost of system (4) in closed loop with (25) is $J^\dagger = w_0^T P^\dagger w_0$, and the cost of (4) with (12) is $J^* = w_0^T P^* w_0$. The proof is completed by selecting $\mu = 1/\lambda_M$, where λ_M is the largest eigenvalue of matrix $P^\dagger(P^*)^{-1}$. □

IV. Experiments Based on Hardware-in-the-Loop Testing

As an experimental method and testing procedure, due to the value that it offers in research, education, and manufacturing, HIL systems have found a wide range of applications in smart grids, power systems, power electronic systems, aircraft and missile industries, automotive industry, motion control, mechatronics, and robotics because of providing ultrahigh-fidelity simulations. The aforementioned experimental methods are currently revolutionizing test engineering in many disciplines, including, but not limited to, smart grids, vehicle and communication systems, civil structures, robotics, aerospace, process control, and naval warships (see [28]–[32] and references therein).

To examine the effectiveness of the proposed primary controller, we have implemented a two-machine MMG on an HIL402 device from Typhoon HIL Inc. [33] and tested the primary controller under the umbrella of smart grids.

It is noteworthy that the system under test here is based on the HIL402's capability of modeling our system, including the proposed controller—thus limiting us to Fig. 1 as the MMG under test. To this end, the abovementioned smart grid employing the suggested primary frequency controller has been examined for investigating its performance under the islanded mode of operation of the formed MMG.

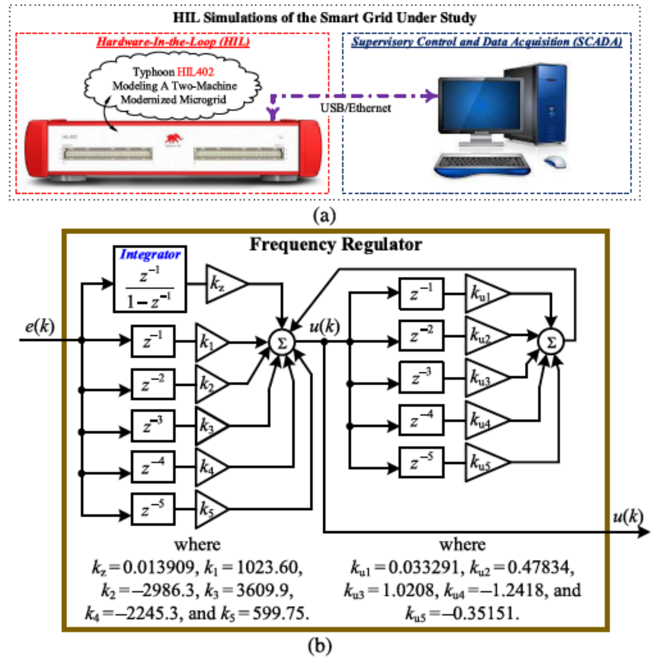

Fig. 3. HIL setup. (a) Employed HIL setup for validations. (b) Structure of the implemented frequency regulator, including controller values.

A. Hardware-in-the-Loop Setup

The complete configuration of the setup is shown in Fig. 3(a). The implemented "frequency regulator," shown in Fig. 2, has been demonstrated in Fig. 3(b).

Typhoon HIL402, with 4 processing cores, 16 analog outputs, 16 digital inputs, and 16-bit resolution, is tailored for the most demanding microgrid and controller test, verification, and precertification tasks. It can test the data-driven algorithm proposed in this article with high fidelity, i.e., 20-ns sampling HIL, and infinitesimal latency, i.e., 1 μs. Indeed, for smart grid testing, HIL402's emulation error and latency are so small that it is difficult to tell the difference between real smart grid and HIL emulator measured waveforms. Moreover, with making use of HIL402, it is possible to simulate our signals with multiple execution rates in a real-time way and improve the overall performance of our HIL testing by maximizing the use of available resources. The built-in multirate interval overrun monitor closely supervises real-time execution and informs the user in case of potential performance issues. This feature is highly required to test the performance of any control algorithm, e.g., the control methodology proposed in this article.

In addition, HIL402 leverages a small simulation time step and advanced numerical algorithms for extremely wide-dynamic-range models. It emulates fast switching dynamics with a simulation time step, as low as 0.5 μs, and has full peace of mind that the part of our model with extremely long time constants will run with high fidelity as well. Indeed,

TABLE I
PARAMETERS OF EACH SET OF ENGINE GENERATORS IN FIG. 1 USED IN HIL VALIDATIONS

Parameter	Value	Parameter	Value
Nominal Power	$1.00\ MVA$	R_s	$9.40 \times 10^{-4}\ \Omega$
Line-to-Line Nominal Voltage	$480.00\ V$	L_{ls}	$1.39 \times 10^{-05}\ H$
Nominal Electrical Frequency	$60.00\ Hz$	L_{md}	$6.53 \times 10^{-4}\ H$
Machine Number of Pole Pairs	2	J_m	$92.88\ kg.m^2$
Actuator gain K	10.00	D	$1.00\ Nms/rad$
Actuator time constant 1; T_{a1}	$2.50 \times 10^{-2}\ s$	L_{mq}	$4.78 \times 10^{-4}\ H$
Actuator time constant 2; T_{a2}	$9.00 \times 10^{-4}\ s$	R_f	$2.16 \times 10^{-4}\ \Omega$
Actuator time constant 3; T_{a3}	$5.74 \times 10^{-3}\ s$	L_{lfd}	$1.42 \times 10^{-4}\ H$
Engine time delay; T_D	$2.40 \times 10^{-2}\ s$	R_{kd}	$4.44 \times 10^{-2}\ \Omega$
Exciter PI proportional gain	2.50×10^{-2}	R_{kq}	$4.00 \times 10^{-3}\ \Omega$
Exciter PI integral gain	7.00×10^{-3}	L_{lkd}	$1.56 \times 10^{-3}\ H$
Exciter time constant; T_e	$1.00 \times 10^{-8}\ s$	L_{lkq}	$9.97 \times 10^{-5}\ H$
Exciter gain; K_e	1.00	N_s/N_{fd}	2.51×10^{-2}
N_s/N_{kd}	1.00	N_s/N_{kq}	1.00

advanced numerical algorithms in HIL402 handle the full dynamic range models masterfully and run them in real time. HIL402 can also automate testing with Python, which is a powerful way of conducting the tests and the ultimate ease of use; it automates controller testing processes with Python scripting and HIL402 platform.

B. Hardware-in-the-Loop Testing

In this section, we apply the proposed adaptive optimal control Algorithm 2 via the structure shown in Fig. 3(b) (including controller settings) for regulating the frequency of the power system shown in Fig. 1. Its parameters have been reported in Table I. For HIL-based experiments in this article, the weight matrices are selected as $Q_1 = 100$, $Q_2 = 10$, and $R = 1$.

The optimal control is computed as follows based on the accurate knowledge of system model:

$$\mathcal{K}^* = [0.1364 \quad -0.3981 \quad 0.4812 \quad -0.2993 \quad 0.0799 \quad 4.439\times10^{-6} \quad 6.377\times10^{-5} \quad 1.36\times10^{-4} \quad -1.656\times10^{-4} \quad -4.687\times10^{-5} \quad 1.855\times10^{-6}].$$

The VI algorithm 2 is tested without the accurate knowledge of the system model. To be more specific, we collect the data along the system trajectory to facilitate the learning of the optimal control gain. The stopping criterion is satisfied after 180 iterations with the corresponding control gain

$$\mathcal{K}_{180} = [0.1291 \quad -0.3768 \quad 0.4556 \quad -0.2835 \quad 0.0757 \quad 4.115\times10^{-6} \quad 6.024\times10^{-5} \quad 1.29\times10^{-4} \quad -1.571\times10^{-4} \quad -4.448\times10^{-5} \quad 1.671\times10^{-6}].$$

The error between $\mathcal{K}_j$ at the jth iteration and its optimal value is shown in Fig. 4. It is checkable that the difference between the learned control gain $\mathcal{K}_j$ and the optimal control gain $\mathcal{K}^*$ is monotonically decreasing as the iteration j increases. The convergence speed of $|\mathcal{K}_j - \mathcal{K}^*|/|\mathcal{K}^*|$ increases in the first 100 iterations and decreases afterward. When the convergence criterion is satisfied, this difference is only 5.67%.

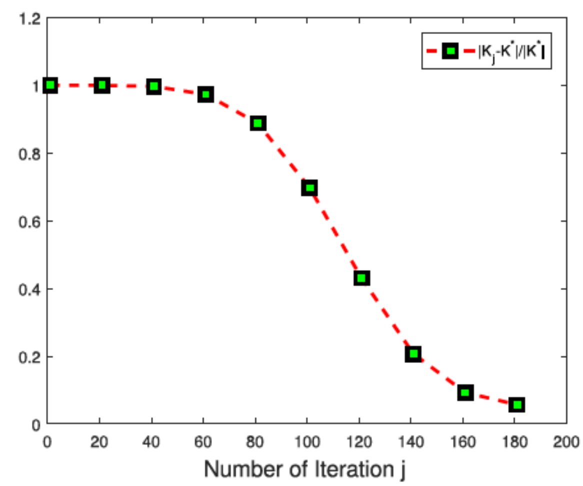

Fig. 4. Comparison of the control gain $\mathcal{K}_j$ with its optimal value $\mathcal{K}^*$.

The HIL test results grained from the MMG system shown in Fig. 1—which is controlled by Fig. 3(b)—have been provided here. Also, for comparison purposes, the responses of the traditional method of the frequency controls in islanded microgrids (i.e., PID controller) have been provided. A tuned PID controller has been employed to conduct the same test cases under which the proposed controller has been examined.

Fig. 5(a) and (b) shows the HIL test results of the so-called “unplanned” islanding testing; in this test, the microgrid has been made islanded without any prior information sent to the system. They mimic the case that microgrid needs to be self-running without being connected to the main utility grid. Fig. 5(a) shows the output of the closed-loop dynamic system [i.e., frequency in per unit (pu)], and Fig. 5(b) shows the input to the plant dynamics [i.e., torque in newton meter (N.m)]—with the horizontal axis of time in second (s).

Also, it is required to check the microgrid’s response when it is in the steady-state condition after getting islanded and see how the demand supply looks like in the steady state. In this regard, the steady-state test case has been conducted, and its

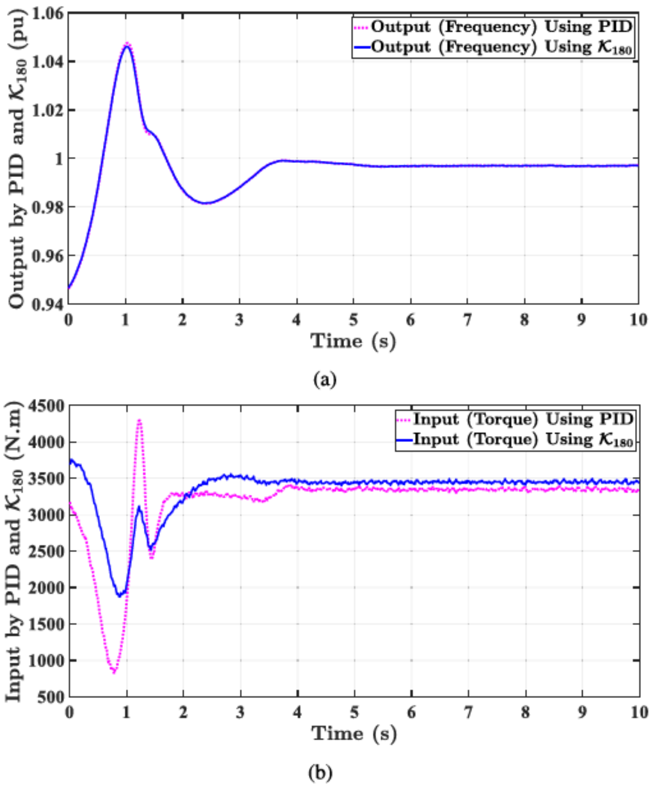

Fig. 5. HIL test results of the so-called "unplanned" islanding testing of the MMG under study controlled by a PID and $\mathcal{K}_{180}$. (a) Output (i.e., frequency) in pu. (b) Input (i.e., torque) in N.m.

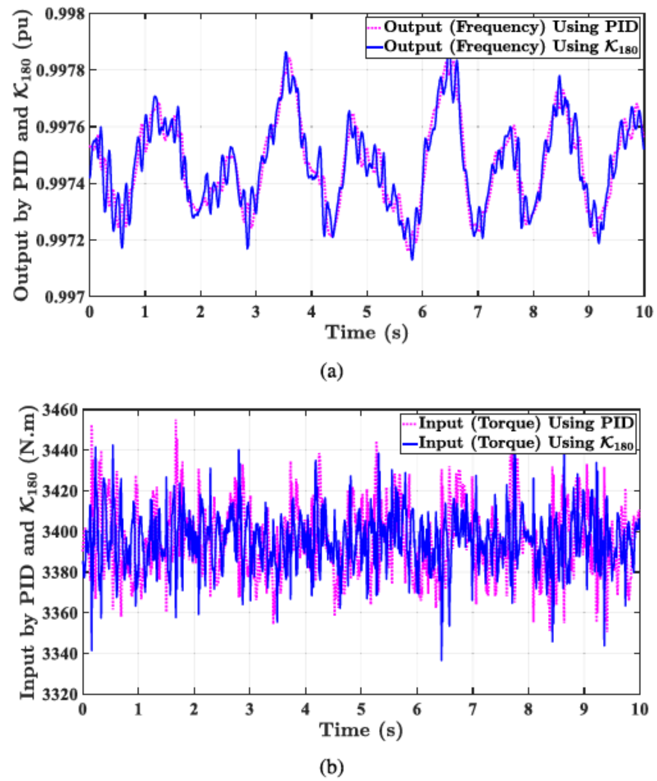

Fig. 6. Steady-state response of the HIL test results of Fig. 5. (a) Output (i.e., frequency) in pu. (b) Input (i.e., torque) in N.m.

results have been shown in Fig. 6(a) and (b). Fig. 6(a) shows the frequency in pu (i.e., the output of the closed-loop dynamic system), and Fig. 5(b) shows the torque in N.m (i.e., the input to the plant dynamics)—with the horizontal axis of time in s.

It is noteworthy that the droop mechanism's impact on the "unplanned" islanding test response has been diminished since we have been interested in rather purely gauging the effect of the primary frequency control loop on frequency dynamics. Thus, equal power share is not evident in Fig. 5. However, the droop mechanism makes the contribution of each engine generator's active power precisely balanced, as it is visible in Fig. 6.

When the microgrid is islanded, its response to load changes should be investigated. In this regard, different loads are connected/disconnected to/from the grid formed. Therefore, both cases of load increase and load decrease need to be studied as they excite the systems differently. As a result, tests shown in Figs. 7 and 8 have been added. Fig. 7 shows the HIL test results associated with the increasing load in the islanded mode. Also, Fig. 8 shows the HIL test related to the decreasing load in the islanded MMG under test—all governed by either the tuned PID controller or $\mathcal{K}_{180}$. Figs. 7(a) and 8(a) show the frequency in pu (i.e., the output), and Figs. 7(b) and 8(b) show the torque in N.m (i.e., the input to the plant dynamics)—with the horizontal axis of time in s.

One can check that, for all these situations, the performance of the proposed optimal controller is better than that of the tuned PID controller. Especially, from the standpoints of the input signal (which is the torque) applied to the

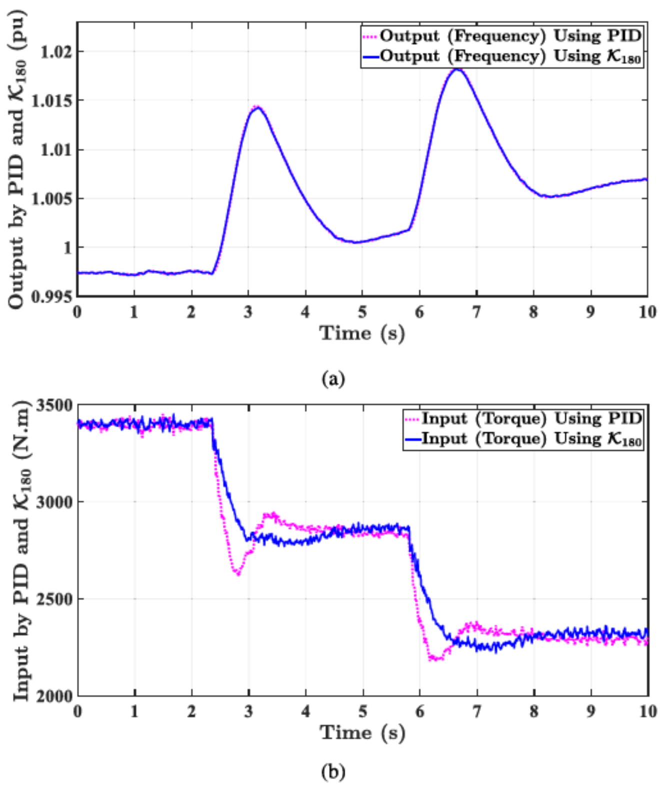

Fig. 7. HIL test results of consecutive step changes in increasing loading of the MMG under test in the islanded mode controlled by PID controller and $\mathcal{K}_{180}$. (a) Output (i.e., frequency) in pu. (b) Input (i.e., torque) in N.m.

system, it is evident that the PID (although tuned) creates overshoot/undershoot torque applied to the system. Note that drastic torques variations and oscillations are not favorable

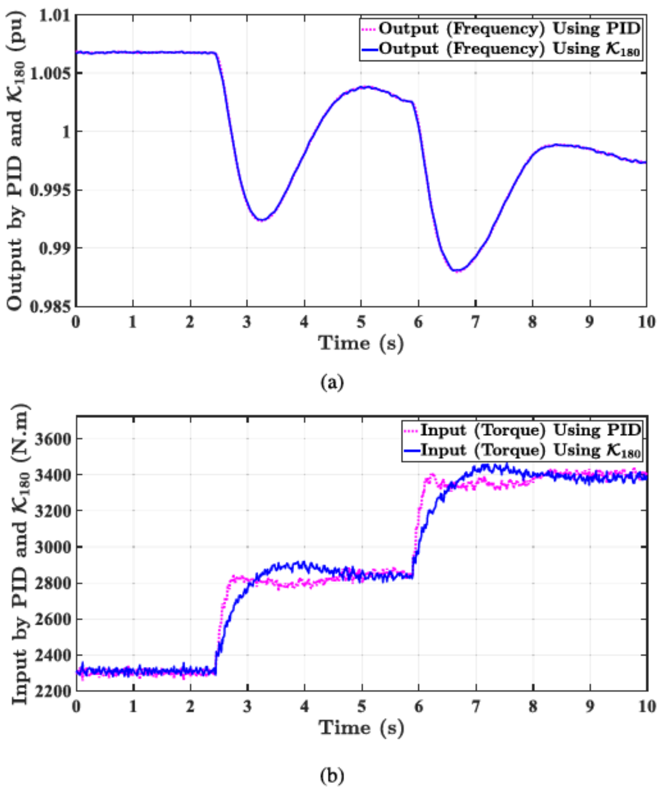

Fig. 8. HIL test results of consecutive step changes in decreasing loading of the MMG under test in the islanded mode controlled by PID controller and $\mathcal{K}_{180}$. (a) Output (i.e., frequency) in pu. (b) Input (i.e., torque) in N.m.

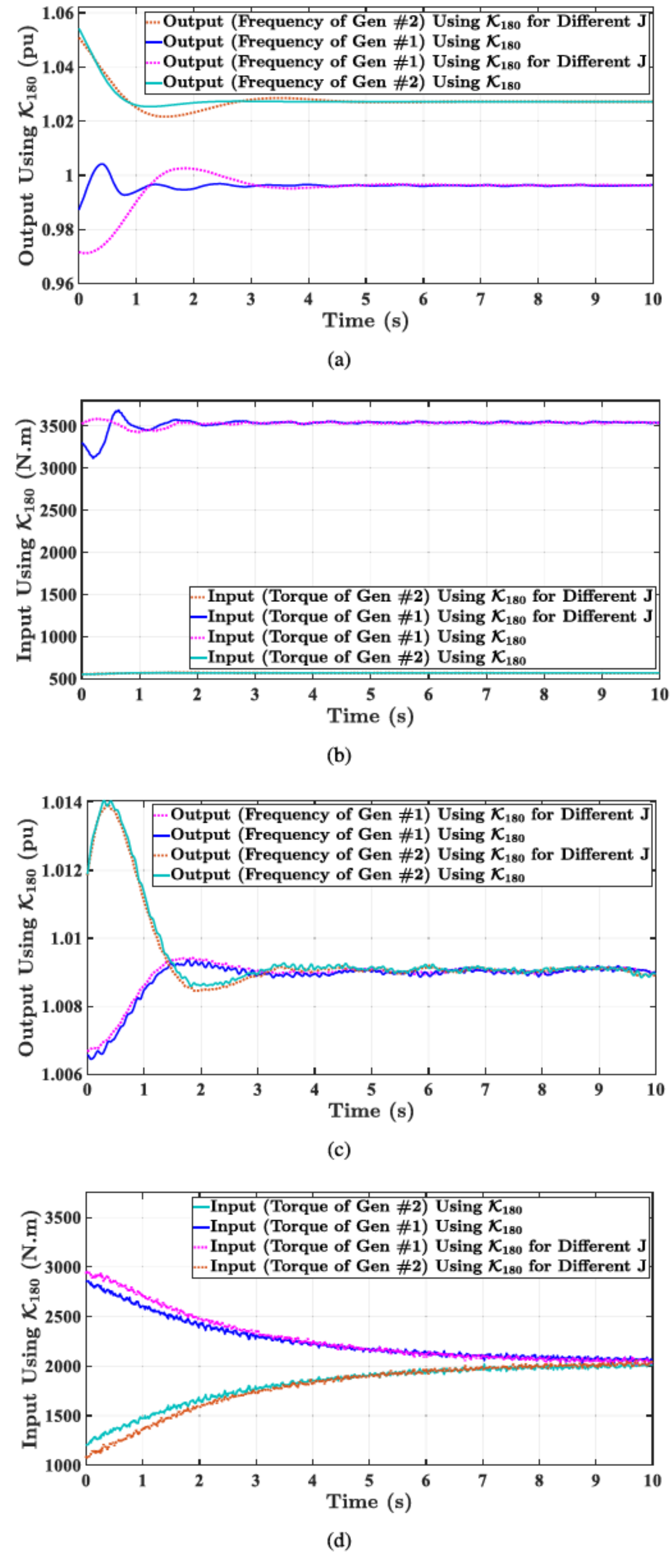

Fig. 9. HIL test results of the MMG under study—controlled by $\mathcal{K}_{\text{final}}$ for the generators with the same J and with the less J (50% less). (a) Output (i.e., frequency) in pu during the "outage" of synchronous generator #2. (b) Input (i.e., torque) in N.m. during the outage. (c) Output in pu during the "reconnection" of synchronous generator #2. (d) Input in N.m. during the reconnection.

(and sometimes not acceptable) in mechanical systems. For example, Fig. 5 shows an unacceptable overshoot/undershoot torque created by the PID controller. This overshoot/undershoot torque is not being made by the proposed controller under both modes of grid-connected and islanded operations. Another significant observation—by comparing Figs. 7 and 8—is that the PID controller cannot behave robustly against load variations. In other words, no matter the system needs to supply either increasing load or decreasing load, the proposed controller has preserved the time response of the closed-loop system.

Besides, another critical test case in the islanded microgrid is when an outage happens. This test is very usual as MMGs may experience generation unit outage—e.g., during fault cases. Regarding this experiment, Fig. 9 shows the response of our proposed control algorithm under the blackout of the synchronous generator #2 shown in Fig. 1, as well as its reconnection. Fig. 9 shows that the proposed controller can stabilize the frequency and power after the outage of one of the generation sources and pick up the load optimally and adequately. Besides, the moment of inertia of machines has been reduced by 50%. Although the system needs to update the gains for finding the best possible optimal gains for the "newly" updated controller, the system time response is acceptable; it looks "semi-"optimal. Undoubtedly, updating the gains can help the time response get closer to the previous one. Finally, after disconnecting synchronous generator #2, the reconnection test case has been applied to the MMG while being controlled by the PID controller for comparison. As expected, the PID controller makes an input that has drastic changes, which are unacceptable for mechanical systems. Fig. 10 has shown this test case, which shows the inefficiency of the PID controller compared with the proposed one.

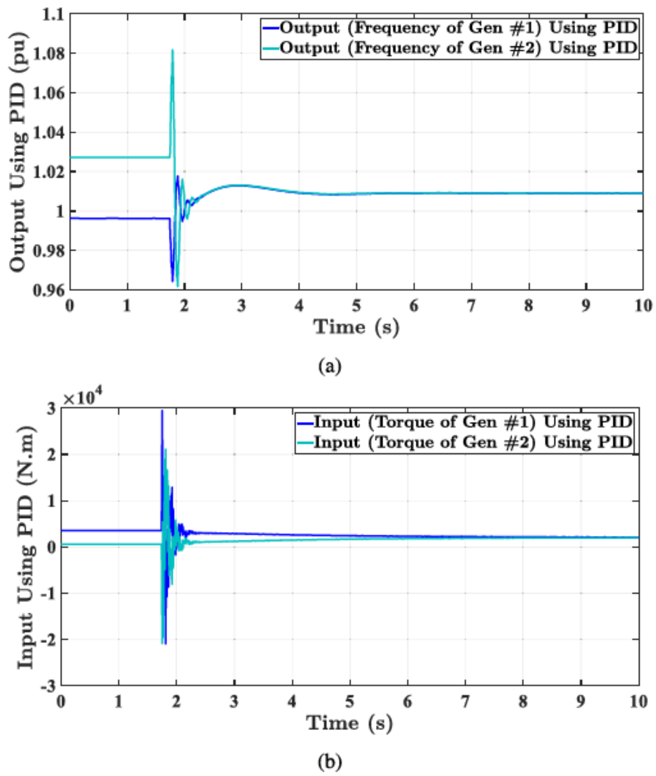

Fig. 10. HIL test results of the "reconnection" of synchronous generator #2 of the MMG under study (after disconnecting it), which is controlled by PID. (a) Output (i.e., frequency) in pu. (b) Input (i.e., torque) in N.m.

Indeed, Figs. 5–10 show the comparison of the PID controller results with the proposed controller outcomes. Those figures have revealed that the performance of the data-driven control is very acceptable from the perspective of the time response compared with a tuned PID controller.

V. Conclusion and Future Work

The primary frequency control of future MMGs is a vital task in the smart grid paradigm, primarily when the MMG is being operated in the islanded mode. Among all entities taking care of primary frequency control, the engine generators are still being employed in many pilot microgrid projects in industrial R&D sections, as well as naval power systems. Challenges associated with this crucial task are as follows: 1) existing uncertainties of the mechanical parameters; 2) the occurrence of uncertain disturbances that are coming from other control loops of electrical variables and uncertainty of loads; 3) operating point variations due to load changes; and 4) last but not least, the appearance of nonminimum phase dynamics associated with the engine delay. This article presents a novel primary frequency control of engine generators of MMGs of the future using measurement feedback control solution to the optimal output regulation of time-delay linear systems with unknown system dynamics and unmeasurable disturbance. An online VI approach is proposed for the design of data-driven adaptive optimal trackers with complete disturbance rejection. HIL-based experiments have been conducted on an MMG using two sets of engine generators in order to validate and examine the effectiveness of the proposed approaches.

In future research, in case more capable real-time simulation platforms (e.g., Typhoon HIL602 and RTDS) are available to us, we will be able to address the optimal control of the MMGs with multiple sources of electric power. Then, we can also consider the power system of more complicated MMGs. Those real-time devices should allow us to implement and examine them in a real-time fashion. Besides, we will target the optimal control for the MMGs' secondary controls. We plan to propose data-driven methods for solving multiobjective optimization problems [34], [35]. We also plan to generalize the presented methodology to nonlinear power systems through the learning-based optimal control framework of [36].

Appendix

Derivation of State-Space Representation

The derivation of the state-space representation of the systems shown in Fig. 2 has been detailed here. Based on Fig. 2, one can find the relation between the output $\omega_r(s)$, the input $u(s)$, and the disturbance $T_e(s)$ in the Laplace domain as follows:

$$\begin{aligned}\omega_r(s) &= \frac{(T_{d1}s+1)(-0.5T_Ds+1)u(s)}{s(T_{d2}s+1)(T_{d3}s+1)(0.5T_Ds+1)(J_ms+D)} - \frac{T_e(s)}{J_ms+D}\\ &= \frac{\beta_{12}s^2+\beta_{11}s+\beta_{10}}{s^5+\alpha_4s^4+\alpha_3s^3+\alpha_2s^2+\alpha_1s}u(s)\\ &\quad+\frac{\beta_{24}s^4+\beta_{23}s^3+\beta_{22}s^2+\beta_{21}s}{s^5+\alpha_4s^4+\alpha_3s^3+\alpha_2s^2+\alpha_1s}T_e(s)\end{aligned} \tag{29}$$

where

$$\begin{aligned}\alpha_4 &= \frac{2J_mT_{2a}T_{3a}+J_mT_{2a}T_D+J_mT_{3a}T_D+DT_{2a}T_{3a}T_D}{J_mT_{2a}T_{3a}T_D}\\ \alpha_3 &= \frac{2J_m(T_{2a}+T_{3a}+T_D/2)}{J_mT_{2a}T_{3a}T_D}+\frac{D(2T_{2a}T_{3a}+(T_{2a}+T_{3a})T_D)}{J_mT_{2a}T_{3a}T_D}\\ \alpha_2 &= \frac{2(J_m+DT_{2a}+DT_{3a})+DT_D}{J_mT_{2a}T_{3a}T_D}\\ \alpha_1 &= \frac{2D}{J_mT_{2a}T_{3a}T_D}\\ \beta_{12} &= \frac{-T_{1a}}{J_mT_{2a}T_{3a}}\\ \beta_{11} &= \frac{2T_{1a}-T_D}{J_mT_{2a}T_{3a}T_D}\\ \beta_{10} &= \frac{2}{J_mT_{2a}T_{3a}T_D}\\ \beta_{24} &= -\frac{1}{J_m}\\ \beta_{23} &= -\frac{2T_{2a}T_{3a}+(T_{2a}+T_{3a})T_D}{J_mT_{2a}T_{3a}T_D}\\ \beta_{22} &= -\frac{2T_{2a}+2T_{3a}+T_D}{J_mT_{2a}T_{3a}T_D}\\ \beta_{21} &= -\frac{2}{J_mT_{2a}T_{3a}T_D}.\end{aligned}$$

One can convert the transfer function to the state-space representation (3) in terms of observable canonical form, where the states are

$$\begin{aligned}
x_5(t) &= \int_0^t \beta_{10} u \, d\tau \\
x_4(t) &= \int_0^t (-\alpha_1 \omega_r + \beta_{11} u + \beta_{21} T_e + x_5) d\tau \\
x_3(t) &= \int_0^t (-\alpha_2 \omega_r + \beta_{12} u + \beta_{22} T_e + x_4) d\tau \\
x_2(t) &= \int_0^t (-\alpha_3 \omega_r + \beta_{23} T_e + x_3) d\tau \\
x_1(t) &= \omega_r(t).
\end{aligned}$$

The corresponding system matrices are

$$\begin{aligned}
A_c &= \begin{bmatrix} -\alpha_4 & 1 & 0 & 0 & 0 \\ -\alpha_3 & 0 & 1 & 0 & 0 \\ -\alpha_2 & 0 & 0 & 1 & 0 \\ -\alpha_1 & 0 & 0 & 0 & 1 \\ 0 & 0 & 0 & 0 & 0 \end{bmatrix}, B_c = \begin{bmatrix} 0 \\ 0 \\ \beta_{12} \\ \beta_{11} \\ \beta_{10} \end{bmatrix}, \quad E_c = \begin{bmatrix} \beta_{24} \\ \beta_{23} \\ \beta_{22} \\ \beta_{21} \\ 0 \end{bmatrix} \\
C &= \begin{bmatrix} -1 & 0 & 0 & 0 & 0 \end{bmatrix}.
\end{aligned}$$

References

[1] F. Katiraei, R. Iravani, N. Hatziargyriou, and A. Dimeas, "Microgrids management: Controls and operation aspects of microgrids," *IEEE Power Energy Mag.*, vol. 6, no. 3, pp. 54–65, Sep. 2008.

[2] M. Davari and Y. A.-R.-I. Mohamed, "Robust multi-objective control of VSC-based DC-voltage power port in hybrid AC/DC multi-terminal micro-grids," *IEEE Trans. Smart Grid*, vol. 4, no. 3, pp. 1597–1612, Sep. 2013.

[3] J. Shiles *et al.*, "Microgrid protection: An overview of protection strategies in north American microgrid projects," in *Proc. IEEE Power Energy Soc. Gen. Meeting*, Jul. 2017, pp. 1–5.

[4] (2007). *Federal Energy Regulatory Commission: Energy Independence and Security Act of 2007 Title XIII Smart Grid*. [Online]. Available: https://www.ferc.gov/industries/electric/indus-act/smart-grid/eisa.pdf

[5] J. W. Simpson-Porco, F. Dörfler, and F. Bullo, "Synchronization and power sharing for droop-controlled inverters in islanded microgrids," *Automatica*, vol. 49, no. 9, pp. 2603–2611, Sep. 2013.

[6] N. Doerry, "Next generation integrated power systems (NGIPS) for the future fleet," in *Proc. IEEE Electr. Ship Technol. Symp.*, Apr. 2009, pp. 200–250.

[7] Q.-C. Zhong and G. Weiss, "Synchronverters: Inverters that mimic synchronous generators," *IEEE Trans. Ind. Electron.*, vol. 58, no. 4, pp. 1259–1267, Apr. 2011.

[8] Q.-C. Zhong, "Virtual synchronous machines: A unified interface for smart grid integration," *IEEE Power Electron. Mag.*, vol. 3, no. 4, pp. 34–43, Dec. 2016.

[9] B. A. Francis and W. M. Wonham, "The internal model principle of control theory," *Automatica*, vol. 12, no. 5, pp. 457–465, Sep. 1976.

[10] A. J. Krener, "The construction of optimal linear and nonlinear regulators," in *Systems, Models and Feedback: Theory and Applications*, vol. 12, A. Isidori and T. J. Tarn, Eds. Boston, MA, USA: Birkhäuser, 1992, pp. 301–322.

[11] Y. Jiang and Z. P. Jiang, *Robust Adaptive Dynamic Programming*. Hoboken, NJ, USA: Wiley, 2017.

[12] F. L. Lewis and D. Vrabie, "Reinforcement learning and adaptive dynamic programming for feedback control," *IEEE Circuits Syst. Mag.*, vol. 9, no. 3, pp. 32–50, Aug. 2009.

[13] W. Gao, Y. Jiang, and M. Davari, "Data-driven cooperative output regulation of multi-agent systems via robust adaptive dynamic programming," *IEEE Trans. Circuits Syst. II, Exp. Briefs*, vol. 66, no. 3, pp. 447–451, Mar. 2019.

[14] X. Zhong, Z. Ni, and H. He, "Gr-GDHP: A new architecture for globalized dual heuristic dynamic programming," *IEEE Trans. Cybern.*, vol. 47, no. 10, pp. 3318–3330, Oct. 2017.

[15] Q.-Y. Fan and G.-H. Yang, "Adaptive actor–critic design-based integral sliding-mode control for partially unknown nonlinear systems with input disturbances," *IEEE Trans. Neural Netw. Learn. Syst.*, vol. 27, no. 1, pp. 165–177, Jan. 2016.

[16] D. Wang, D. Liu, H. Li, B. Luo, and H. Ma, "An approximate optimal control approach for robust stabilization of a class of discrete-time nonlinear systems with uncertainties," *IEEE Trans. Syst., Man, Cybern. Syst.*, vol. 46, no. 5, pp. 713–717, May 2016.

[17] W. Gao and Z.-P. Jiang, "Adaptive dynamic programming and adaptive optimal output regulation of linear systems," *IEEE Trans. Autom. Control*, vol. 61, no. 12, pp. 4164–4169, Dec. 2016.

[18] H. Li, D. Liu, and D. Wang, "Integral reinforcement learning for linear continuous-time zero-sum games with completely unknown dynamics," *IEEE Trans. Autom. Sci. Eng.*, vol. 11, no. 3, pp. 706–714, Jul. 2014.

[19] Q. Wei and D. Liu, "Adaptive dynamic programming for optimal tracking control of unknown nonlinear systems with application to coal gasification," *IEEE Trans. Autom. Sci. Eng.*, vol. 11, no. 4, pp. 1020–1036, Oct. 2014.

[20] W. Gao, Z.-P. Jiang, F. L. Lewis, and Y. Wang, "Leader-to-formation stability of multiagent systems: An adaptive optimal control approach," *IEEE Trans. Autom. Control*, vol. 63, no. 10, pp. 3581–3587, Oct. 2018.

[21] H. Modares and F. L. Lewis, "Linear quadratic tracking control of partially-unknown continuous-time systems using reinforcement learning," *IEEE Trans. Autom. Control*, vol. 59, no. 11, pp. 3051–3056, Nov. 2014.

[22] E. Johansson, "Detailed description of synchronous machine models used in Simpow," M.S. thesis, Dept. Elect. Eng., Roy. Inst. Technol. Sweden-KTH, Stockholm, Sweden, 2002.

[23] S. J. Soras, "Frequency regulation of synchronous generator," M.S. thesis, Geophys. Inst., Univ. Bergen, Bergen, Norway, Jun. 2017.

[24] P. C. Krause, O. Wasynczuk, S. D. Sudhoff, and S. Pekarek, "Synchronous machines," in *Analysis of Electric Machinery and Drive Systems*. Hoboken, NJ, USA: Wiley, 2013, ch. 5, pp. 142–214.

[25] T. Chen and B. A. Francis, *Optimal Sampled-Data Control Systems*. London, U.K.: Springer, 1995.

[26] J. Huang, *Nonlinear Output Regulation: Theory and Applications*. Philadelphia, PA, USA: SIAM, 2004.

[27] P. Lancaster and L. Rodman, *Algebraic Riccati Equations*. New York, NY, USA: Oxford Univ. Press, 1995.

[28] S. H. Mousavi, M. Davari, and H. J. Marquez, "An innovative event-based filtering scheme using H_∞ performance for stochastic LTI systems considering a practical application in smart modernized microgrids," *IEEE Access*, vol. 7, pp. 48138–48150, Apr. 2019.

[29] P. E. Pace, M. D. Nash, D. P. Zulaica, A. A. Di Mattesa, and A. Hosmer, "Relative targeting architectures for captive-carry HIL missile simulator experiments," *IEEE Trans. Aerosp. Electron. Syst.*, vol. 37, no. 3, pp. 810–823, Jul. 2001.

[30] dSPACE GmbH (LLC). *HIL Testing System*. Accessed: Dec. 5, 2019. [Online]. Available: https://www.dspace.com/en/pub/home/products/systems/ecutest.cfm

[31] M. Davari and F. Katiraei, "Investigation and correction of phase shift delays in power hardware in loop real-time digital simulation testing of power electronic converters," in *Proc. Grid Future Symp. (CIGRE US Nat. Committee)*, Oct. 2015, pp. 1–11. [Online]. Available: http://cigre-usnc.tamu.edu/wp-content/uploads/2015/10/DAVARI.pdf

[32] M. Davari, "Dynamics of an industrial power amplifier for evaluating PHIL testing accuracy: An experimental approach via linear system identification methods," in *Proc. IEEE Int. Conf. Ind. Electron. for Sustain. Energy Syst. (IESES)*, Jan. 2018, pp. 540–545.

[33] *Typhoon HIL Inc. HIL402*. Accessed: Mar. 4, 2020. [Online]. Available: https://www.typhoon-hil.com/products/hil402

[34] C. Yin, T. Xue, X. Huang, Y.-H. Cheng, S. Dadras, and S. Dadras, "Research on damages evaluation method with multi-objective feature extraction optimization scheme for M/OD impact risk assessment," *IEEE Access*, vol. 7, pp. 98530–98545, 2019.

[35] C. Yin, S. Dadras, X. Huang, Y. Chen, and S. Zhong, "Optimizing energy consumption for lighting control system via multivariate extremum seeking control with diminishing dither signal," *IEEE Trans. Autom. Sci. Eng.*, vol. 16, no. 4, pp. 1848–1859, Oct. 2019.

[36] W. Gao and Z.-P. Jiang, "Learning-based adaptive optimal tracking control of strict-feedback nonlinear systems," *IEEE Trans. Neural Netw. Learn. Syst.*, vol. 29, no. 6, pp. 2614–2624, Jun. 2018.

Masoud Davari (Senior Member, IEEE) was born in Isfahan, Iran, in September 1985. He received the B.Sc. degree (Hons.) in electrical engineering–power from the Isfahan University of Technology, Isfahan, in September 2007, the M.Sc. degree (Hons.) in electrical engineering–power from the Amirkabir University of Technology (Tehran Polytechnic), Tehran, Iran, in January 2010, and the Ph.D. degree in electrical engineering–energy systems from the University of Alberta, Edmonton, AB, Canada, in January 2016.

He was with Iran's Grid Secure Operation Research Center and Iran's Electric Power Research Institute (EPRI), Tehran, from January 2010 to December 2011. From April 2015 to June 2017, he has been collaborating with Quanta-Technology Company, Markham, ON, Canada, in the field of the dynamic interaction of renewable energy systems with smart grids as well as control, protection, and automation of microgrids as a Senior Research and Development Specialist and a Senior Consultant. In July 2017, he joined the Department of Electrical and Computer Engineering, Allen E. Paulson College of Engineering and Computing, Georgia Southern University, Statesboro, GA, USA, as a tenure-track Assistant Professor. He has developed and implemented several experimental test rigs for both research universities and the industry. He has also authored several IEEE TRANSACTIONS and journals. His research interests include the dynamics, controls, and protections of different types of power electronic converters, which are employed in the hybrid ac/dc smart grids, and hardware-in-the-loop (HIL) testing of modernized power systems.

Dr. Davari is an invited member of the Golden Key International Honor Society. He has been serving as an active member and a Chapter Lead (for Chapter 3) at the IEEE WG P2004, a newly established IEEE working group on the HIL simulation for IEEE Standards Association, since June 2017. He received the Best Reviewer of the IEEE TRANSACTIONS ON POWER SYSTEMS in 2018. He served as the Chair of the Literature Review Subgroup of DC@home Standards for the IEEE Standards Association from April 2014 to October 2015. He is also the invited reviewer for several IEEE TRANSACTIONS and journals, IET journals, *Energies*, and various IEEE conferences, as well as the invited speaker at different universities and in diverse societies.

Weinan Gao (Member, IEEE) received the B.Sc. degree in automation and the M.Sc. degree in control theory and control engineering from Northeastern University, Shenyang, China, in 2011 and 2013, respectively, and the Ph.D. degree in electrical engineering from New York University, Brooklyn, NY, USA, in 2017.

He is currently an Assistant Professor of electrical and computer engineering with the Allen E. Paulson College of Engineering and Computing, Georgia Southern University, Statesboro, GA, USA. His research interests include reinforcement learning, adaptive dynamic programming (ADP), optimal control, cooperative adaptive cruise control (CACC), intelligent transportation systems, sampled-data control systems, and output regulation theory.

Dr. Gao was a recipient of the Best Paper Award at the IEEE International Conference on Real-Time Computing and Robotics (RCAR) in 2018 and the David Goodman Research Award at New York University in 2019. He serves as an Associate Editor for *Neurocomputing* and a member of the Editorial Board of *Neural Computing and Applications*.

Zhong-Ping Jiang (Fellow, IEEE) received the B.Sc. degree in mathematics from Wuhan University, Wuhan, China, in 1988, the M.Sc. degree in statistics from the University of Paris XI, Paris, France, in 1989, and the Ph.D. degree in automatic control and mathematics from the Mines ParisTech, Paris, in 1993, under the direction of Prof. L. Praly.

He is currently a Professor of electrical and computer engineering with the Tandon School of Engineering, New York University, Brooklyn, NY, USA. He is the coauthor of four books: *Stability and Stabilization of Nonlinear Systems* (with Dr. I. Karafyllis, Springer, 2011), *Nonlinear Control of Dynamic Networks* (with Dr. T. Liu and Dr. D. J. Hill, Taylor & Francis, 2014), *Robust Adaptive Dynamic Programming* (with Y. Jiang, Wiley-IEEE Press, 2017), and *Nonlinear Control Under Information Constraints* (with T. Liu, Science Press, 2018). His main research interests include stability theory, robust/adaptive/distributed nonlinear control, learning-based control, adaptive dynamic programming, and their applications to information, mechanical, and biological systems.

Dr. Jiang is a fellow of the International Federation of Automatic Control (IFAC) and a Clarivate Analytics Highly Cited Researcher. He is also a Deputy Co-Editor-in-Chief of the *Journal of Control and Decision* and the IEEE/CAA JOURNAL OF AUTOMATICA SINICA. He has served as a Senior Editor for the IEEE CONTROL SYSTEMS LETTERS and the *Systems and Control Letters* and an associate editor for several journals.

Frank L. Lewis (Life Fellow, IEEE) received the bachelor's degree in physics and electrical engineering and the M.S.E.E. degree from Rice University, Houston, TX, USA, in 1971, the M.S. degree in aeronautical engineering from the University of West Florida, Pensacola, FL, USA, in 1977, and the Ph.D. degree in electrical engineering from the Georgia Institute of Technology, Atlanta, GA, USA, in 1981.

He is currently a Distinguished Scholar Professor and a Distinguished Teaching Professor with The University of Texas at Arlington, Fort Worth, TX, USA, and the Moncrief-O'Donnell Chair of the University of Texas at Arlington Research Institute. He has authored 6 U.S. patents, numerous journal special issues, journal articles, and 20 books, including *Optimal Control* (Wiley), *Aircraft Control* (Wiley), *Optimal Estimation* (Wiley), and *Robot Manipulator Control* (CRC Press), which are used as university textbooks worldwide. He is also a UTA Distinguished Scholar Professor, a UTA Distinguished Teaching Professor, and the Moncrief-O'Donnell Chair at The University of Texas at Arlington Research Institute. He works in feedback control, intelligent systems, cooperative control systems, and nonlinear systems. He is the author of 7 U.S. patents, numerous journal special issues, 420 journal articles, and 20 books, including the textbooks *Optimal Control, Aircraft Control, Optimal Estimation* and *Robot Manipulator Control*. His research interests include feedback control, intelligent systems, cooperative control systems, and nonlinear systems.

Dr. Lewis is a member of the National Academy of Inventors, a fellow of the International Federation of Automatic Control (IFAC), the American Association for the Advancement of Science (AAAS), and the U.K. Institute of Measurement and Control, a PE of Texas, and a U.K. Chartered Engineer. He received the Fulbright Research Award, the NSF Research Initiation Grant, the Terman Award from the American Society for Engineering Education (ASEE), the Gabor Award from the International Neural Network Society, the Honeywell Field Engineering Medal from the U.K. Institute of Measurement and Control, the Neural Networks Pioneer Award from the IEEE Computational Intelligence Society, the Intelligent Systems Award from AIAA, and the Ragazzini Award from the American Automatic Control Council (AACC).